Published June 20, 2019

Original Research

Core Ideas

- Conventional methods for measuring CEC are time consuming and costly.
- A Vis–NIRS model and pedotransfer function (PTF) were developed for CEC determination.
- The Vis–NIRS model estimated CEC accurately for different soil types.
- The Vis–NIRS CEC model performed better than the PTF based on clay and organic C contents.

Comparison of Cation Exchange Capacity Estimated from Vis–NIR Spectral Reflectance Data and a Pedotransfer Function

Hafeez Ur Rehman,* Maria Knadel, Lis W. de Jonge, Per Moldrup, Mogens H. Greve, and Emmanuel Arthur

Knowledge of the cation exchange capacity (CEC) for soils or other porous media is very important for civil engineering and agricultural applications. However, the standard laboratory methods to measure CEC are costly and laborious. The aim of this research was to develop a visible–near-infrared spectroscopy (Vis–NIRS, 400–2500 nm) calibration model to predict CEC based on multivariate analysis and to compare the predictive ability of Vis–NIRS with that of a pedotransfer function (PTF). For this purpose, reference CEC was measured by the ammonium acetate method for 235 soil samples, collected from 21 countries. Diffuse spectral reflectance data were also collected by using a NIRSTM DS2500 spectrometer. The model was constructed on a calibration subset (80%) and evaluated with a validation subset (20%) using partial least squares regression. The Vis–NIRS calibration model was sufficiently robust based on the cross-validation results [R^2 = 0.79, RMSE of cross-validation values of 7.9 $cmol_c\ kg^{-1}$ and bias = −0.14]. The independent validation of the Vis–NIRS model showed good prediction accuracy, regardless of sample origin (RMSE of prediction value of 5.0 $cmol_c\ kg^{-1}$ and ratio of performance to interquartile distance value of 4.5). Moreover, the Vis–NIRS prediction performance was superior to that of the PTF, which was influenced by the sample origin (RMSE values of 11.5 $cmol_c\ kg^{-1}$). The better prediction of CEC by the Vis–NIRS calibration model suggests that it is due to the co-variation of CEC with clay (type and content) and organic C content.

Abbreviations: CEC, cation exchange capacity; OC, organic carbon; OM, organic matter; PLSR, partial least squares regression; PTF, pedotransfer function; RMSEC, root mean square error of calibration; RMSECV, root mean square error of cross-validation; RMSEP, root mean square error of prediction; RPIQ, the ratio of performance to interquartile distance; Vis–NIR, visible–near-infrared; Vis–NIRS, visible–near-infrared spectroscopy.

H.U. Rehman, M. Knadel, L.W. de Jonge, M.H. Greve, and E. Arthur, Dep. of Agroecology, Faculty of Science and Technology, Aarhus Univ., Blichers Allé 20, PO Box 50, DK-8830 Tjele, Denmark; P. Moldrup, Dep. of Civil Engineering, Aalborg Univ., Thomas Manns Vej 23, DK-9220 Aalborg, Denmark. *Corresponding author (hafeez@agro.au.dk, hafeezrehman2011@hotmail.com).

Received 29 Oct. 2018.
Accepted 4 Mar. 2019.
Supplemental material online.

Citation: Rehman, H.U., M. Knadel, L.W. de Jonge, P. Moldrup, M.H. Greve, and E. Arthur. 2019. Comparison of cation exchange capacity estimated from Vis–NIR spectral reflectance data and a pedotransfer function. Vadose Zone J. 18:180192. doi:10.2136/vzj2018.10.0192

Cation exchange capacity (CEC) is a vital soil property that plays an important role in filtration of water, provision of food and fiber, and soil swell and shrinkage potential. The CEC is an essential soil property required in national or global soil databases because it is significant in decision making in agronomy, environmental management, and geotechnical applications (Janzen, 2004; Khorshidi and Lu, 2017; Yilmaz, 2004). In agronomy and environmental management, CEC is crucially important for soil fertility, nutrient dynamics, and hydraulic conductivity (Noble et al., 2000; Środoń and McCarty, 2008; Stockmann et al., 2015). For many geotechnical applications, CEC and clay content and type are required for preliminary design estimates and assessment of the swelling potential of clays (Yilmaz, 2004; Yukselen-Aksoy and Kaya, 2006).

Conventional methods for determining CEC comprise the ammonium acetate (Sumner and Miller, 1996), the barium chloride (Bascomb, 1964), or the ammonium chloride methods (Schollenberger and Dreibelbis, 1930). Drawbacks of these methods are that they are costly and time-consuming for a large number of samples. To combat these challenges, several pedotransfer functions (PTFs) have been developed to predict CEC from easily measured soil properties. The consistency of PTFs is mainly dependent on the number of samples and range of the input parameters (Chirico et al., 2010). Pedotransfer functions for CEC are often developed from a combination of different properties (e.g., clay content, organic C [OC] content, and hygroscopic water content) (Arthur,

2017; Krogh et al., 2000; McBratney et al., 2002; Olorunfemi et al., 2016; Torrent et al., 2015). For instance, Krogh et al. (2000) showed that a PTF based on clay and OM contents dominated by illite reliably explained 90% of the variability in CEC for Danish soils. Similarly, McBratney et al. (2002) also showed that a PTF based on clay and OC explained 73% of the variability in CEC.

An alternative method for predicting CEC is the application of visible–near-infrared diffuse reflectance spectroscopy (Vis–NIRS: range from 400 to 2500 nm). The use of Vis–NIRS has shown great potential for estimating several soil physical, chemical, and hydraulic properties and some biological properties due to its simplicity, rapidity, nondestructiveness, and cost-effective analysis (Babaeian et al., 2015; Hermansen et al., 2017; Rossel et al., 2006; Santra et al., 2009; Soriano-Disla et al., 2014; Stenberg et al., 2010). Previous local studies have successfully estimated CEC using Vis–NIRS for samples from specific geographic areas. For example, Pinheiro et al. (2017) used 434 Brazilian samples and reported good prediction performance of Vis–NIRS for CEC (range: 1 to 69 $cmol_c\ kg^{-1}$) (RMSE of prediction [RMSEP] = 5.86 $cmol_c\ kg^{-1}$). Similar prediction performance was also reported for CEC for 50 Californian and 330 Turkish soils (Ulusoy et al., 2016; van Groenigen et al., 2003). Prediction of soil properties with Vis–NIRS from a specific geographic area often produces better results than predictions from different geographic areas, due to similar soil mineralogical composition and specific spectra measurement protocols and spectral analysis in a region of interest (Horta et al., 2015). Further, developing multivariate calibrations is important to reduce the calibration errors for a large number of samples having large variability (Stevens et al., 2013). To the best of our knowledge, no studies of Vis–NIRS measurement of CEC of soils from different geographic origins have yet been presented in the literature. The objectives of the study were (i) to develop a Vis–NIRS calibration model to predict CEC for soil samples collected from different geographical regions, and (ii) to compare the predictive ability of the Vis–NIRS CEC calibration with a newly developed PTF based on clay and OC contents.

Materials and Methods

Soil Sampling

To account for regional variability in the samples used for the study, we collected 235 soil samples from different parts of the world (Fig. 1). The samples were collected from Western and Northern Europe (108), North America (75), South America (14), Africa (31), and Asia (7). The dataset covered a wide range of soil texture classes from clay to sand (Fig. 1).

Laboratory Analysis

The soil samples were air dried, ground to pass a 2-mm sieve, and analyzed in a laboratory for CEC, clay, silt, sand, and OC contents. Cation exchange capacity was determined through extraction in ammonium acetate at pH 7 for the majority of the samples and at pH 8.2 for 25 samples (Sumner and Miller, 1996). The particle size distribution was determined by the wet

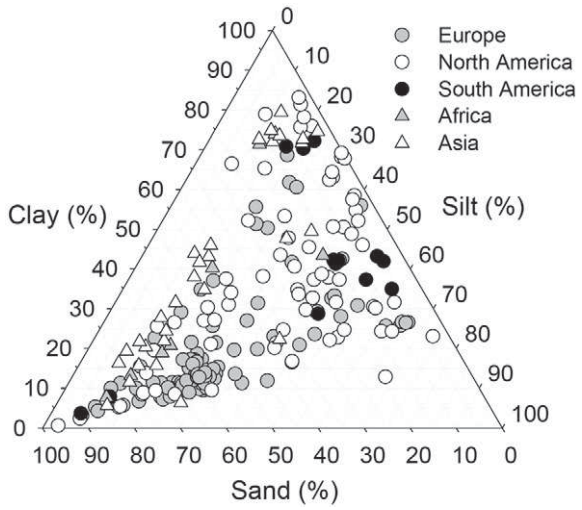

Fig. 1. Distribution of soil samples in the USDA soil texture triangle.

sieving, pipette, and hydrometer method as described in Gee and Or (2002) after removal of organic matter (OM) and carbonates. The total C content was determined on ball-milled samples with an organic elemental analyzer coupled to a thermal conductivity detector (Thermo Fisher Scientific) by the oxidation of C at 1800°C. Total C equaled OC unless a preceding test indicated the presence of carbonates. For samples containing carbonates, OC was the difference between total C and inorganic C calculated from the $CaCO_3$ percentage. For 60 of the samples, OM was determined by the Walkley–Black method (Nelson and Sommers, 1996) and then converted to OC by assuming that 58% of OM is OC (Warington and Peake, 1880).

Vis–NIRS Measurements

The 2-mm sieved and air-dried samples were scanned in the laboratory (average temperature = 24°C and relative humidity = 62.4% during the scanning) using a commercially available Vis–NIR spectrometer, NIRSTM DS2500 (FOSS). The spectrometer was equipped with Si (400–1100 nm) and PbS (1100–2500 nm) detectors. The instrument covered a spectral range between 400 and 2500 nm with a spectral resolution of 8.75-nm full width at half height and a sampling interval of 0.5 nm. Prior to the measurements, the instrument was calibrated using white reference (Spectralon). When calculating relative reflectance, the digital number of the sample was ratioed against the digital number of the white reference. Approximately 50 g of soil was placed in a 7-cm sample cup equipped with a 6-cm quartz window at the bottom. Reflectance was collected at seven spots of the sample cup and the average spectrum was extracted for each sample for further analysis. The reflectance measurements were converted to absorbance by $A = [\log(R^{-1})]$, where R is the reflectance.

Multivariate Data Analysis

Before developing Vis–NIRS calibration model for CEC, the dataset of 235 samples was divided into calibration and validation

subsets. The split was done automatically with the onion algorithm (Sousa et al., 2015) in the PLS Toolbox 8.2 software (Eigenvector Research) into two subsets: 80% (188 samples) for calibration and 20% (47 samples) assigned to a validation subset to assess the models' performance. The onion splitting method first selects a ring of the unique samples according to CEC range (based on distance from the mean—like the outermost layer of an onion); these are placed in the calibration set. Second, a ring of less unique CEC samples, just inside the first set (the next onion layer), is put into the validation set. This is repeated two more times, so there are three outer rings of the most unique and less unique samples. Finally, all remaining samples are split randomly into the calibration and validation subsets.

Partial least square regression (PLSR) has become a preferred method for constructing predictive Vis–NIRS models (Feyziyev et al., 2016; Ulusoy et al., 2016; van Groenigen et al., 2003; Waruru et al., 2015). We applied PLSR by using Unscrambler X 10.5 software (Camo ASA) to model the relationship between the reference CEC data and the Vis–NIR absorbance spectral data. Before PLSR analysis, preprocessing techniques such as smoothing, derivatives, standard normal variate (SNV), baseline, and normalization were tested. Due to the fine resolution of the spectra, pre-processing techniques had no impact on the calibration models and the raw absorbance spectral data were used in the development of the calibration models. The calibration model was validated using a leave-one-out full cross-validation method resulting in estimation of CEC for all 188 samples.

Development of Pedotransfer Function

To compare the performance of the Vis–NIRS calibration model to PTF prediction, the calibration dataset was also used to develop a PTF based on clay and OC content. A brief description of the PTF is

$$\mathrm{CEC} = 0.60 + (0.61 \times \mathrm{Clay}) + (2.00 \times \mathrm{OC}) \quad (p \text{ value} < 0.001;\ \text{adjusted } R^2 = 0.53;\ \mathrm{SEE} = 11.9) \quad [1]$$

where CEC is in centimoles of charge per kilogram, clay and OC contents are in mass percent, and SEE is the standard error of the estimate.

The prediction of CEC for the validation dataset was then used to compare the performance of the PTF to that of the Vis–NIRS calibration model.

Evaluation of Model Performance

To evaluate the predictive ability of the Vis–NIRS model and PTF, the RMSE of calibration (RMSEC), the RMSE of cross-validation (RMSECV), and the value of the squared Pearson correlation coefficient (R^2) were used. To evaluate the independent validation, the RMSE of prediction (RMSEP), and the ratio of performance to interquartile distance (RPIQ) were additionally used. The model was ranked by RPIQ as a measure of the goodness of the calibration model (Bellon-Maurel et al., 2010). The RMSE and RPIQ are calculated as

$$\mathrm{RMSE} = \sqrt{\sum \frac{(\mathrm{CEC_e} - \mathrm{CEC_r})^2}{N}} \quad [2]$$

where $\mathrm{CEC_e}$ and $\mathrm{CEC_r}$ are the estimated and reference values of CEC, and N is the number of samples, and

$$\mathrm{RPIQ} = \frac{\mathrm{IQ}}{\mathrm{RMSEP}} = \frac{\mathrm{Q3} - \mathrm{Q1}}{\mathrm{RMSEP}} \quad [3]$$

where IQ is the interquartile distance that gives the range that accounts for 50% of the population around the median, Q1 is where 25% of the samples can be found, and Q3 is where 75% of the samples can be found.

The range of measured values of the considered soil property influences the RMSE strongly. Thus, to compare the performance of the model to other studies where RPIQ is not available, the standardized RMSE (SRMSE) was used:

$$\mathrm{SRMSE} = \mathrm{RMSE}/\mathrm{Range} \quad [4]$$

where Range represents the difference between the smallest and largest values of CEC for the respective dataset or from published studies. Smaller SRMSE values denote better predictions and vice versa.

Results and Discussion

Soil Properties

The descriptive statistics of the particle size distribution, OC, and CEC of the investigated samples are presented in Table 1, and an overview of their distribution in the USDA texture triangle is illustrated in Fig. 1. The soil samples are distributed across the texture classes from clay to sand; silt was the only texture class with no samples. The soil samples exhibited a wide range in CEC (1–83

Table 1. General statistics of soil texture, organic C (OC), and cation exchange capacity (CEC) for the entire dataset (n = 235) and calibration (n = 188) and validation (n = 47) subsets.

Property	Mean	Min.	Max.	SD	Q1†	Q3†
Clay, %	30 (30, 28)‡	1 (2, 1)	83 (83, 75)	21 (21, 20)	1 (13, 13)	42 (42, 42)
Silt, %	29 (29, 29)	3 (7, 3)	73 (73, 62)	14 (15, 13)	3 (18, 19)	39 (39, 37)
Sand, %	41 (41, 43)	0 (0, 0)	96 (91, 96)	25 (26, 25)	0 (16, 24)	61 (61, 60)
OC, %	1.69 (1.76, 1.41)	0.03 (0.03, 0.10)	8.42 (8.42, 4.48)	1.38 (1.45, 1.0)	0.03 (0.69, 0.77)	2.26 (2.37, 1.94)
CEC, $\mathrm{cmol_c\ kg^{-1}}$	23 (22, 23)	1 (1, 2)	83 (83, 83)	18 (17, 20)	1 (11, 10)	31 (31, 33)

† Q1, first quartile; Q3, third quartile.
‡ The first value is for the entire dataset, the first value in parentheses is for the calibration subset, and the second value in parentheses is for the validation subset.

$cmol_c\ kg^{-1}$), clay content (1–83%), and OC content (0.03–8.42%). Differences in the sample origin are evident in the variability in the clay mineral composition as well. The samples were dominated by kaolinites (~12%), smectites (~25%), illites and micas (~13%), or a mixture of two or more of these three minerals and traces of vermiculite (~50%). The variability in the properties and the clay mineral composition was very important for developing models that have wider applicability than local models. Supplemental information on the soil properties for each sample is provided in Supplemental Table S1.

General Characterization of the Vis–NIR Spectra

The distinct differences in spectral signatures among three-selected soil samples with identical clay content (~43%) but different clay mineralogy (illitic, kaolinitic, and smectitic) are presented in Fig. 2. The different clay minerals in soils show diagnostic absorption in the Vis–NIR range. These absorption bands caused by vibrational transitions commonly display sharp and narrow features (Zheng et al., 2016) (Fig. 2). The selected smectitic sample from Texas, USA, shows large CEC values (43.3 $cmol_c\ kg^{-1}$) and display distinct spectral features. The absorption bands near ~1400 nm (overtones caused by O-H stretch in its octahedral layer), ~1900 nm (overtones caused by molecular water), and ~2200 nm (combination vibration of water bound in the interlayer lattice) (Bishop et al., 1994; Post and Noble, 1993) are very pronounced and clear. The illite minerals are typically formed in colder regions (Ben-Dor, 2002). Here, the illite-rich soil sample is from Denmark with CEC of 16.2 $cmol_c\ kg^{-1}$. It shows a more pronounced absorption feature near 1900 nm, related to OH bonds and two very weak absorption near 1400 and 2200 nm, all common for illite minerals (Stenberg et al., 2010). A kaolinitic sample is represented by a Nigerian soil with CEC of 5.2 $cmol_c\ kg^{-1}$. It shows very pronounced absorption peaks near 1400 and 1900 nm related to OH bonds (Clark, 1999; Post and Noble, 1993). The observed peak near 2200 nm is a result of a combination of Al-OH bending and O-H stretch (Bishop et al., 1994; Clark et al., 1990; Post and Noble, 1993). The Nigerian sample shows spectral doublet near 2200 nm. Moreover, it shows the highest absorption feature in the visible range. The typical convex spectral feature near 500 nm is also observed here and is related to the presence of OM (Ben-Dor, 2002). An additional absorption band near 920 nm indicates the presence of Fe oxide mineral (goethite) (Scheinost et al., 1998).

The CEC is more related to clay minerals than the total amount of clay. This can also be seen in the spectra. Even though all three soils contained the same amount of clay (~43%), they had significantly different CEC values, and the response related to the different minerals was also clear in the Vis–NIR spectra.

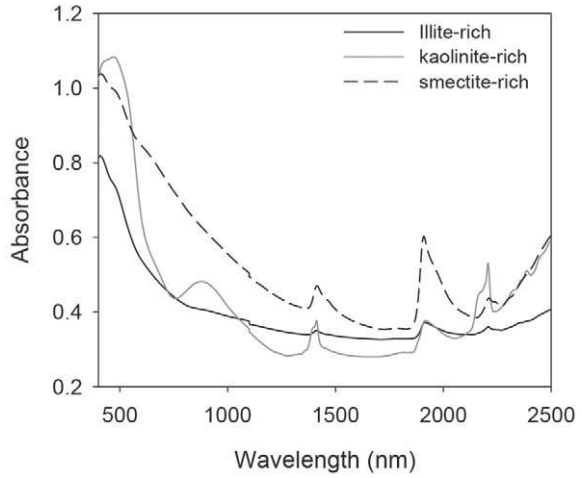

Fig. 2. Example of visible–near-infrared (Vis–NIR) spectra for an illite-rich (Denmark), kaolinite-rich (Nigeria), and smectite-rich (Texas) soil samples.

Vis–NIRS Calibration Model and Independent Validation

CEC Calibration Model

A successful calibration model for CEC using Vis–NIR spectra and seven factors was obtained after the regression analyses (Supplemental Table S2). The R^2, RMSEC, and bias of the calibration model were 0.83, 6.99 and 0.00 $cmol_c\ kg^{-1}$, respectively. As illustrated in Fig. 3, the performance of the calibration model after cross-validation was very good (R^2 = 0.79, bias = −0.14, and RMSECV and SRMSE of 7.89 $cmol_c\ kg^{-1}$ and 0.10, respectively). This is in agreement with previous studies where the performance of CEC calibration models, after cross-validation, was excellent. For example, studies by Waruru et al. (2014), Ulusoy et al. (2016), and Shepherd and Walsh (2002) reported R^2 > 0.80 and SRMSE values ranging from 0.05 to 0.09. Even though CEC is not spectrally active in the Vis–NIR range, it reflects the OM content, clay mineral types, and clay content of the samples—three properties that are expressed strongly in the Vis–NIR spectra (Dalal and Henry, 1986; Soriano-Disla et al., 2014; Viscarra Rossel et al., 2006). It is therefore probable that the obtained strong relationship between Vis–NIR spectra and the CEC content emanates from

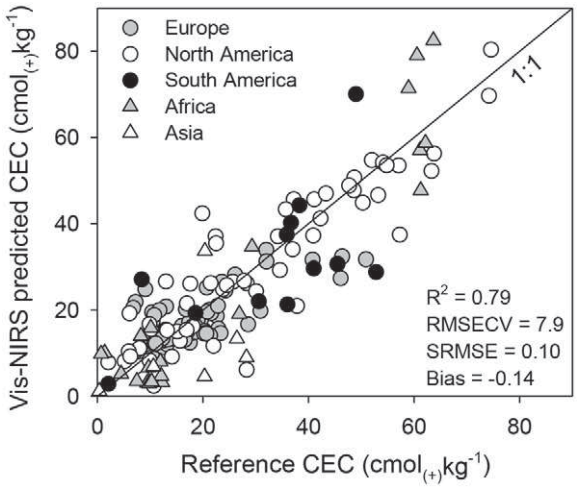

Fig. 3. Results of a leave-one-out full cross-validation of the cation exchange capacity (CEC) calibration model. RMSECV, RMSE of cross-validation; SRMSE, standardized RMSE (RMSE/$Range_{CEC}$, where $Range_{CEC}$ is the range in values for CEC).

the dependence of CEC on other spectrally active soil properties. Thus, the correlations between Vis–NIR spectra with clay and OC on the exact same calibration set were also tested. One needs to keep in mind, however, that the three properties represent different ranges and units. Thus, a direct comparison is difficult. Moreover, the caveat with this comparison is the inherent assumption that the accuracy and error associated with the laboratory measurement of the three properties is similar. Clearly higher accuracy for CEC (calibration: $R^2 = 0.83$, RMSEC = 6.99 $cmol_c\ kg^{-1}$ and cross-validation: $R^2 = 0.79$, RMSECV = 7.89 $cmol_c\ kg^{-1}$) than for clay (calibration: $R^2 = 0.69$, RMSEC = 11.73% and cross-validation: $R^2 = 0.65$, RMSECV = 12.57%) and OC contents (calibration: $R^2 = 0.57$, RMSEC = 0.95% and cross-validation: $R^2 = 0.53$, RMSECV = 0.99%) using Vis–NIRS-derived calibration, and cross-validated models were found. The calibration and cross-validation results suggest a combined contribution of both mineral and organic spectral responses for CEC determination. To confirm this joined contribution, the regression coefficients of the Vis–NIR calibration model of CEC were compared with and superimposed on those of clay and OC models.

Regression Coefficients

The regression coefficients from the calibration PLSR analysis for CEC, clay, and OC contents are shown in Fig. 4. Multiple wavelengths important for the CEC determination are present in the regression coefficient across visible and NIR spectral range and can be related to both soil mineral and organic components. In the visible range, there is a high and negative regression coefficient near 500 nm that nearly overlaps with a regression coefficient from the OC model. The absorptions in this region are usually assigned to Fe oxides as the possible components (Sherman, 1985). Further, two less important coefficients near 610 and 780 nm are present and are overlapping with more pronounced coefficients from OC and clay, respectively. Absorption features near 620 nm were previously reported to be related to Fe oxides in goethite and hematite, but the region between 570 and 700 nm was also assigned to OM (Galvdo et al., 1997; Stenberg et al., 2010). No possible component responsible for the absorptions near 780 nm was found in the literature; however, amine (N-H) and aromatics (C-H) were previously found to contribute to absorptions at 751 and 825 nm (Clark et al., 1990). Thus, this region is most likely related to OM.

The most important wavelengths for CEC determination in the NIR region are located near 1400, 1900, and 2200 nm. The negative regression coefficient at 1400 nm is present for all three properties and is related to the first overtone of O-H stretch in its octahedral layer of clay minerals. Absorptions near 1900 nm are related to OH and the combination vibrations of water bound in the interlayer lattice (Bishop et al., 1994). Here, a positive regression coefficient for both CEC and clay and a negative for OC can be seen. At ~2200 nm, a high and negative regression coefficient for CEC is present and is of much higher intensity than that of OC, which was most likely decreased due to higher absorption near 2100 nm (assigned to OM) (Ben-Dor et al., 1997). A positive

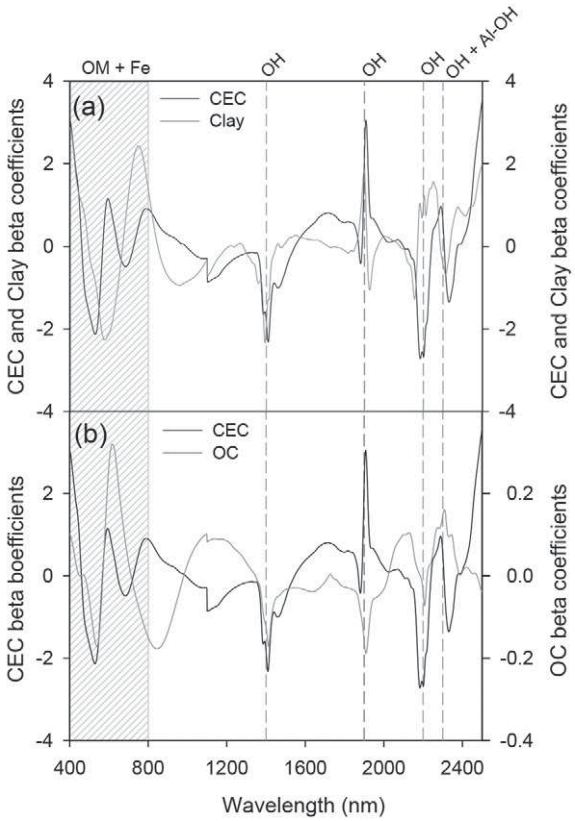

Fig. 4. The comparison between the regression coefficients of calibration models for (a) cation exchange capacity (CEC) and clay content, and (b) CEC and organic C (OC) content.

regression coefficient can be seen in region of 2200 nm and is assigned to Al-OH bend with O-H stretch combinations typical for clay minerals.

Less important regression coefficients at 2280 (Ben-Dor et al., 1997) and 2300 nm (Mg-OH) (Clark et al., 1990) can be also noticed for the CEC and are overlapping with OC and clay regression coefficients near 2210 nm (Al–OH bend and O–H stretch combination) (Clark et al., 1990) and 2308 nm (aliphatic C–H stretch) (Ben-Dor et al., 1997), respectively. The analysis of regression coefficients confirmed that the determination of CEC was enabled through its co-variation with both clay and OC, and what is explained by the good correlation with clay and OC contents (Eq. [1]) and regression coefficients.

CEC Independent Validation

The independent validation of the calibration model, presented in Fig. 5a, showed very good prediction accuracy ($R^2 = 0.94$, RMSEP = 5.01 $cmol_c\ kg^{-1}$, SRMSE = 0.06, and RPIQ = 4.50). Generally, the prediction of CEC from Vis–NIRS in the literature shows high predictive accuracy. Rossel et al. (2016) provided an overview of the CEC prediction performance of 26 studies with an average R^2 and RMSE of 0.73 (0.43–0.90) and 3.80 $cmol_c\ kg^{-1}$ (1.00–9.60), respectively. The CEC-independent validation results presented here showed better accuracy than some studies that used datasets with less variable samples from local datasets or

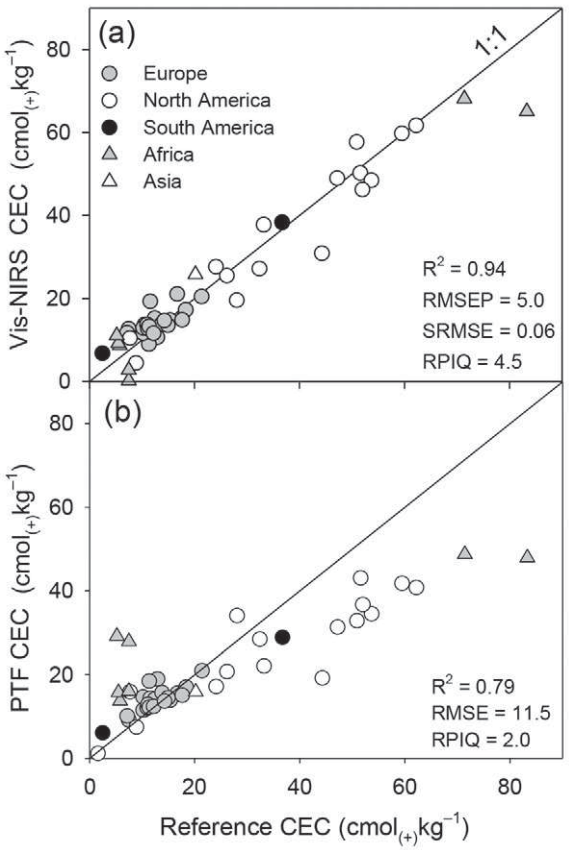

Fig. 5. Scatterplot of (a) measured cation exchange capacity (CEC) content compared with visible–near-infrared spectroscopy (Vis–NIRS) estimated CEC for independent soil samples, and (b) measured CEC content compared with CEC estimated from a pedotransfer function (PTF), developed based on the calibration dataset. RMSEP, RMSE of prediction; SRMSE, standardized RMSE (RMSE/$Range_{CEC}$, where $Range_{CEC}$ is range in values for CEC); RPIQ, ratio of performance to interquartile range.

from one geographical region. For instance, Pinheiro et al. (2017) reported less accurate CEC prediction for Brazilian soil samples with R^2 = 0.68, SRMSE = 0.09, and RPIQ = 0.82; Waruru et al. (2014) estimated CEC for 120 samples from Kenya and reported R^2 = 0.70 and SRMSE = 0.13; and Leone et al. (2012) achieved R^2 = 0.70 and SRMSE = 0.08 for 124 samples from Italy. The less accurate prediction of the spectroscopic models for CEC reported in previous studies can be attributed to a lower variability or smaller CEC range in the soil samples used for calibration. Results better than and/or comparable with those of our study were reported by Nduwamungu et al. (2009), who used 150 Canadian samples and reported CEC prediction accuracy of R^2 = 0.89 and SRMSE = 0.10. Similarly, Vendrame et al. (2012) obtained R^2 of 0.81 and SRMSE of 0.05 for 148 Brazilian samples.

Comparison of Vis–NIRS and Pedotransfer Functions for CEC Prediction

The tedious nature of conventional measurement methods for CEC precipitated the development of PTFs that are based on easily measureable soil properties (e.g., clay and OC). The comparison of the PTF developed in this study and Vis–NIRS in predicting CEC is shown in Fig. 5a and 5b. The European samples (composed primarily of illite or a mixture of different clay minerals) and samples with CEC <40 $cmol_c\ kg^{-1}$ were well-estimated by the PTF. Conversely, samples with CEC >40 $cmol_c\ kg^{-1}$ were consistently underestimated, and some African samples (dominated by kaolinite mineral) with the lowest CEC were overestimated by PTF and well estimated by Vis–NIR. The Vis–NIRS CEC prediction performance was significantly better (R^2 = 0.94 and RPIQ = 4.5, and RMSE = 5.01 $cmol_c\ kg^{-1}$) than that of the PTF (R^2 = 0.79, RPIQ = 2.2, and RMSE = 11.5 $cmol_c\ kg^{-1}$) and showed good predictions for all the samples regardless of the magnitude of CEC or origin.

Conclusions

Visible–NIRS was successfully used to predict CEC using a set of soil samples from different geographic regions. The estimated CEC was in good agreement with the measured values (RMSE of 5.01 $cmol_c\ kg^{-1}$). A successful independent CEC validation was achieved (RPIQ = 4.5) and was better than the estimation of clay and OC contents (RPIQ of 3.9 and 2.0, respectively). It was attributed to a high correlation of CEC to C and clay contents, as well as to mineralogy, and was well reflected in the CEC regression coefficient indicating the joint contribution of both the organic and mineral composition in predicting the CEC values.

Evaluation of a newly developed PTF to estimate CEC revealed fair estimations, though the estimations were affected by the range of CEC. The Vis–NIRS approach was superior to that of PTF and was not affected by the sample origin or range of CEC values. Thus, it can be inferred that Vis–NIRS could be used as a fast alternative method for estimating CEC for variable soils with a wide range of CEC and originating from different geographic areas, whereas PTFs may be better for local scale estimations.

Supplemental Material

The supplemental material includes information regarding geographical origin, clay, silt, sand, organic C, and CEC of the investigated soil samples. Additionally, it contains the CEC calibration models for use and validation by other researchers.

Acknowledgments

This research was financed by VILLUM FONDEN Research Grant 13162. We especially thank Dr. Cristine Morgan, formerly of Texas A&M University, and the International Soil Reference and Information Centre (ISRIC) for providing soil samples for the research.

References

Arthur, E. 2017. Rapid estimation of cation exchange capacity from soil water content. Eur. J. Soil Sci. 68:365–373. doi:10.1111/ejss.12418

Babaeian, E., M. Homaee, H. Vereecken, C. Montzka, A.A. Norouzi, and M.Th. van Genuchten. 2015. A comparative study of multiple approaches for predicting the soil–water retention curve: Hyperspectral information vs. basic soil properties. Soil Sci. Soc. Am. J. 79:1043–1058. doi:10.2136/sssaj2014.09.0355

Bascomb, C.L. 1964. Rapid method for the determination of cation-exchange capacity of calcareous and non-calcareous soils. J. Sci. Food Agric. 15:821–823. doi:10.1002/jsfa.2740151201

Bellon-Maurel, V., E. Fernandez-Ahumada, B. Palagos, J.M. Roger, and A. McBratney. 2010. Critical review of chemometric indicators commonly used for assessing the quality of the prediction of soil attributes by NIR spectroscopy. Trends Anal. Chem. 29:1073–1081. doi:10.1016/j.trac.2010.05.006

Ben-Dor, E. 2002. Quantitative remote sensing of soil properties. In: D.L. Sparks, editor, Advances in agronomy. Acad. Press, Cambridge, MA. Vol. 75. p. 173-243.

Ben-Dor, E., Y. Inbar, and Y. Chen. 1997. The reflectance spectra of organic matter in the visible near-infrared and short wave infrared region (400–2500 nm) during a controlled decomposition process. Remote Sens. Environ. 61:1–15. doi:10.1016/S0034-4257(96)00120-4

Bishop, J.L., C.M. Pieters, and J.O. Edwards. 1994. Infrared spectroscopic analyses on the nature of water in montmorillonite. Clays Clay Miner. 42:702–716. doi:10.1346/CCMN.1994.0420606

Chirico, G.B., H. Medina, and N. Romano. 2010. Functional evaluation of PTF prediction uncertainty: An application at hillslope scale. Geoderma 155:193–202. doi:10.1016/j.geoderma.2009.06.008

Clark, R.N. 1999. Spectroscopy of rocks and minerals, and principles of spectroscopy. In: A.N. Rencz, editor, Manual of remote sensing, Vol. 3. Remote sensing for earth sciences. 3rd ed. John Wiley & Sons, Hoboken, NJ. p. 3–52.

Clark, R.N., T.V.V. King, M. Klejwa, G.A. Swayze, and N. Vergo. 1990. High spectral resolution reflectance spectroscopy of minerals. J. Geophys. Res. 95(B8):12653–12680. doi:10.1029/JB095iB08p12653

Dalal, R.C., and R.J. Henry. 1986. Simultaneous determination of moisture, organic carbon, and total nitrogen by near infrared reflectance spectrophotometry. Soil Sci. Soc. Am. J. 50:120–123. doi:10.2136/sssaj1986.03615995005000010023x

Feyziyev, F., M. Babayev, S. Priori, and G. L'Abate. 2016. Using visible-near infrared spectroscopy to predict soil properties of Mugan Plain, Azerbaijan. Open J. Soil Sci. 6:52–58. doi:10.4236/ojss.2016.63006

Galvdo, L.S., Í. Vitorello, and A.R. Formaggio. 1997. Relationships of spectral reflectance and color among surface and subsurface horizons of tropical soil profiles. Remote Sens. Environ. 61:24–33. doi:10.1016/S0034-4257(96)00219-2

Gee, G.W., and D. Or. 2002. Particle-size analysis. In: J.H. Dane and G.C. Topp, editors, Methods of soil analysis. Part 4. SSSA Book Ser. 5. SSSA, Madison, WI. p. 255–293. doi:10.2136/sssabookser5.4.c12

Hermansen, C., M. Knadel, P. Moldrup, M.H. Greve, D. Karup, and L.W. de Jonge. 2017. Complete soil texture is accurately predicted by visible near-infrared spectroscopy. Soil Sci. Soc. Am. J. 81:758–769. doi:10.2136/sssaj2017.02.0066

Horta, A., B. Malone, U. Stockmann, B. Minasny, T.F.A. Bishop, A.B. McBratney, et al. 2015. Potential of integrated field spectroscopy and spatial analysis for enhanced assessment of soil contamination: A prospective review. Geoderma 241–242:180–209. doi:10.1016/j.geoderma.2014.11.024

Janzen, H.H. 2004. Carbon cycling in earth systems: A soil science perspective. Agric. Ecosyst. Environ. 104:399–417. doi:10.1016/j.agee.2004.01.040

Khorshidi, M., and N. Lu. 2017. Determination of cation exchange capacity from soil water retention curve. J. Eng. Mech. 143(6). doi:10.1061/(ASCE)EM.1943-7889.0001220

Krogh, L., H. Breuning-Madsen, and M.H. Greve. 2000. Cation-exchange capacity pedotransfer functions for Danish soils. Acta Agric. Scand., Sect. B 50:1–12. doi:10.1080/090647100750014358

Leone, A.P., R.A. Viscarra-Rossel, P. Amenta, and A. Buondonno. 2012. Prediction of soil properties with PLSR and vis-NIR spectroscopy: Application to Mediterranean soils from southern Italy. Curr. Anal. Chem. 8:283–299. doi:10.2174/157341112800392571

McBratney, A.B., B. Minasny, S.R. Cattle, and R.W. Vervoort. 2002. From pedotransfer functions to soil inference systems. Geoderma 109:41–73. doi:10.1016/S0016-7061(02)00139-8

Nduwamungu, C., N. Ziadi, G.F. Tremblay, and L.E. Parent. 2009. Near-infrared reflectance spectroscopy prediction of soil properties: Effects of sample cups and preparation. Soil Sci. Soc. Am. J. 73:1896–1903. doi:10.2136/sssaj2008.0213

Nelson, D.W., and L.E. Sommers. 1996. Total carbon, organic carbon, and organic matter. In: D.L. Sparks, editor, Methods of soil analysis. Part 3. Chemical methods. SSSA and ASA, Madison, WI. p. 961–1010. doi:10.2136/sssabookser5.3.c34

Noble, A.D., G.P. Gillman, and S. Ruaysoongnern. 2000. A cation exchange index for assessing degradation of acid soil by further acidification under permanent agriculture in the tropics. Eur. J. Soil Sci. 51:233–243. doi:10.1046/j.1365-2389.2000.00313.x

Olorunfemi, I.E., J.T. Fasinmirin, and A.S. Ojo. 2016. Modeling cation exchange capacity and soil water holding capacity from basic soil properties. Eurasian Soil Sci. 4:266–274. doi:10.18393/ejss.2016.4.266-274

Pinheiro, E.F.M., M.B. Ceddia, C.M. Clingensmith, S. Grunwald, and G.M. Vasques. 2017. Prediction of soil physical and chemical properties by visible and near-infrared diffuse reflectance spectroscopy in the central Amazon. Remote Sens. 9(4):293. doi:10.3390/rs9040293

Post, J.L., and P.N. Noble. 1993. The near-infrared combination band frequencies of dioctahedral smectites, micas, and illites. Clays Clay Miner. 41:639–644. doi:10.1346/CCMN.1993.0410601

Rossel, R.A.V., T. Behrens, E. Ben-Dor, D.J. Brown, J.A.M. Dematte, K.D. Shepherd, et al. 2016. A global spectral library to characterize the world's soil. Earth Sci. Rev. 155:198–230. doi:10.1016/j.earscirev.2016.01.012

Rossel, R.A.V., D.J.J. Walvoort, A.B. McBratney, L.J. Janik, and J.O. Skjemstad. 2006. Visible, near infrared, mid infrared or combined diffuse reflectance spectroscopy for simultaneous assessment of various soil properties. Geoderma 131:59–75. doi:10.1016/j.geoderma.2005.03.007

Santra, P., R.N. Sahoo, B.S. Das, R.N. Samal, A.K. Pattanaik, and V.K. Gupta. 2009. Estimation of soil hydraulic properties using proximal spectral reflectance in visible, near-infrared, and shortwave-infrared (VIS–NIR–SWIR) region. Geoderma 152:338–349. doi:10.1016/j.geoderma.2009.07.001

Scheinost, A., A. Chavernas, V. Barrón, and J. Torrent. 1998. Use and limitations of second-derivative diffuse reflectance spectroscopy in the visible to near-infrared range to identify and quantity Fe oxide minerals in soils. Clays Clay Miner. 46:528–536. doi:10.1346/CCMN.1998.0460506

Schollenberger, C.J., and F.R. Dreibelbis. 1930. Analytical methods in base exchange investigations on soils. Soil Sci. 30:161–174. doi:10.1097/00010694-193009000-00001

Shepherd, K.D., and M.G. Walsh. 2002. Development of reflectance spectral libraries for characterization of soil properties. Soil Sci. Soc. Am. J. 66:988–998. doi:10.2136/sssaj2002.9880

Sherman, D.M. 1985. Electronic spectra of Fe^{3+} oxides and oxide hydroxides in the near IR to near UV. Am. Mineral. 70:1262–1269.

Soriano-Disla, J.M., L.J. Janik, R.A.V. Rossel, L.M. Macdonald, and M.J. McLaughlin. 2014. The performance of visible, near-, and mid-infrared reflectance spectroscopy for prediction of soil physical, chemical, and biological properties. Appl. Spectrosc. Rev. 49:139–186. doi:10.1080/05704928.2013.811081

Sousa, A.G., L.I. Ahl, H.L. Pedersen, J.U. Fangel, S.O. Sørensen, and W.G.T. Willats. 2015. A multivariate approach for high throughput pectin profiling by combining glycan microarrays with monoclonal antibodies. Carbohydr. Res. 409:41–47. doi:10.1016/j.carres.2015.03.015

Środoń, J., and D.K. McCarty. 2008. Surface area and layer charge of smectite from CEC and EGME/H_2O-retention measurements. Clays Clay Miner. 56:155–174. doi:10.1346/CCMN.2008.0560203

Stenberg, B., R.A.V. Rossel, A.M. Mouazen, and J. Wetterlind. 2010. Visible and near infrared spectroscopy in soil science. Adv. Agron. 107:163–215. doi:10.1016/S0065-2113(10)07005-7

Stevens, A., M. Nocita, G. Tóth, L. Montanarella, and B. van Wesemael. 2013. Prediction of soil organic carbon at the European scale by visible and near Infrared reflectance spectroscopy. PLoS One 8:e66409. doi:10.1371/journal.pone.0066409

Stockmann, U., J. Padarian, A. McBratney, B. Minasny, D. de Brogniez, L. Montanarella, et al. 2015. Global soil organic carbon assessment. Global Food Secur. 6:9–16. doi:10.1016/j.gfs.2015.07.001

Sumner, M.E., and W.P. Miller. 1996. Cation exchange capacity and exchange coefficients. In: D.L. Sparks, editor, Methods of soil analysis. Part 3. Chemical methods. SSSA and ASA, Madison, WI. p. 1201–1229. doi:10.2136/sssabookser5.3.c40

Torrent, J., M.C. Del Campillo, and V. Barron. 2015. Predicting cation exchange capacity from hygroscopic moisture in agricultural soils of Western Europe. Span. J. Agric. Res. 13(4):e11SC01. doi:10.5424/sjar/2015134-8212

Ulusoy, Y., Y. Tekin, Z. Tumsavas, and A.M. Mouazen. 2016. Prediction of soil cation exchange capacity using visible and near infrared spectroscopy. Biosyst. Eng. 152:79–93. doi:10.1016/j.biosystemseng.2016.03.005

van Groenigen, J.W., C.S. Mutters, W.R. Horwath, and C. van Kessel. 2003. NIR and DRIFT-MIR spectrometry of soils for predicting soil and crop parameters in a flooded field. Plant Soil 250:155–165. doi:10.1023/A:1022893520315

Vendrame, P.R.S., R.L. Marchao, D. Brunet, and T. Becquer. 2012. The potential of NIR spectroscopy to predict soil texture and mineralogy in Cerrado Latosols. Eur. J. Soil Sci. 63:743–753. doi:10.1111/j.1365-2389.2012.01483.x

Viscarra Rossel, R.A., D.J.J. Walvoort, A.B. McBratney, L.J. Janik, and J.O. Skjemstad. 2006. Visible, near infrared, mid infrared or combined diffuse reflectance spectroscopy for simultaneous assessment of various soil properties. Geoderma 131:59–75. doi:10.1016/j.geoderma.2005.03.007

Warington, R., and W.A. Peake. 1880. On the determination of carbon in soils. J. Chem. Soc. 37:617–625.

Waruru, B.K., K.D. Shepherd, G.M. Ndegwa, P.T. Kamoni, and A.M. Sila. 2014. Rapid estimation of soil engineering properties using diffuse reflectance near infrared spectroscopy. Biosyst. Eng. 121:177–185. doi:10.1016/j.biosystemseng.2014.03.003

Waruru, B.K., K.D. Shepherd, G.M. Ndegwa, A. Sila, and P.T. Kamoni. 2015. Application of mid-infrared spectroscopy for rapid characterization of key soil properties for engineering land use. Soils Found. 55:1181–1195. doi:10.1016/j.sandf.2015.09.018 [erratum: 55(6):1520].

Yilmaz, I. 2004. Relationships between liquid limit, cation exchange capacity, and swelling potentials of clayey soils. Eurasian Soil Sci. 37:506–512.

Yukselen-Aksoy, Y., and A. Kaya. 2006. Prediction of cation exchange capacity from soil index properties. Clay Miner. 41:827–837. doi:10.1180/0009855064140222

Zheng, G., C. Jiao, S. Zhou, and G. Shang. 2016. Analysis of soil chronosequence studies using reflectance spectroscopy. Int. J. Remote Sens. 37:1881–1901. doi:10.1080/01431161.2016.1163751